



# Marine $^{187}\text{Os}/^{188}\text{Os}$ isotope stratigraphy reveals the interaction of volcanism and ocean circulation during Oceanic Anoxic Event 2



Alice D.C. Du Vivier<sup>a,\*</sup>, David Selby<sup>a</sup>, Bradley B. Sageman<sup>b</sup>, Ian Jarvis<sup>c</sup>, Darren R. Gröcke<sup>a</sup>, Silke Voigt<sup>d</sup>

<sup>a</sup> Department of Earth Sciences, Durham University, Durham DH1 3LE, UK

<sup>b</sup> Department of Geological Sciences, Northwestern University, Evanston, IL 60208, USA

<sup>c</sup> School of Geography, Geology and the Environment, Kingston University London, Kingston upon Thames KT1 2EE, UK

<sup>d</sup> Institute of Geosciences, Goethe-University Frankfurt, Altenhöferallee 1, 60438 Frankfurt, Germany

## ARTICLE INFO

### Article history:

Received 5 July 2013

Received in revised form 10 December 2013

Accepted 17 December 2013

Available online 6 January 2014

Editor: G. Henderson

### Keywords:

OAE 2

$^{187}\text{Os}/^{188}\text{Os}$  isotope composition

palaeocirculation

global warming

Caribbean LIP

carbon

## ABSTRACT

High-resolution osmium (Os) isotope stratigraphy across the Cenomanian–Turonian Boundary Interval from 6 sections for four transcontinental settings has produced a record of seawater chemistry that demonstrates regional variability as a function of terrestrial and hydrothermal inputs, revealing the impact of palaeoenvironmental processes. In every section the  $^{187}\text{Os}/^{188}\text{Os}$  profiles show a comparable trend; radiogenic values in the lead up to Oceanic Anoxic Event 2 (OAE 2); an abrupt unradiogenic trend at the onset of OAE 2; an unradiogenic interval during the first part of OAE 2; and a return to radiogenic values towards the end of the event, above the Cenomanian–Turonian boundary. The unradiogenic trend in  $^{187}\text{Os}/^{188}\text{Os}$  is synchronous in all sections. Previous work suggests that activity of the Caribbean LIP (Large Igneous Province) was the source of unradiogenic Os across the OAE 2 and possibly an instigator of anoxia in the oceans. Here we assess this hypothesis and consider the influence of activity from other LIPs; such as the High Arctic LIP.

A brief shift to high radiogenic  $^{187}\text{Os}/^{188}\text{Os}$  values occurred in the Western Interior Seaway before the onset of OAE 2. We evaluate this trend and suggest that a combination of factors collectively played critical roles in the initiation of OAE 2; differential input of nutrients from continental and volcanogenic sources, coupled with efficient palaeocirculation of the global ocean and epeiric seas, enhanced productivity due to higher nutrient availability, which permitted penecontemporaneous transport of continental and LIP-derived nutrients to trans-equatorial basins.

© 2013 The Authors. Published by Elsevier B.V. This is an open access article under the CC BY license (<http://creativecommons.org/licenses/by/3.0/>).

## 1. Introduction

The Cenomanian–Turonian boundary (CTB) OAE 2 records an extensive period of global anoxia, represented worldwide by sections containing organic-rich marine sedimentary rocks. Strata marking the onset of OAE 2 are globally correlated by a 2 to 4‰ positive excursion in the carbon stable isotope composition of organic matter ( $\delta^{13}\text{C}_{\text{org}}$ ) and marine carbonates ( $\delta^{13}\text{C}_{\text{carb}}$ ), which are interpreted to reflect the onset of massive organic carbon burial and widespread oxygen deficiency in the oceans (Jenkyns, 1980; Schlanger et al., 1987). The OAE 2 has been studied using numerous proxies (e.g. carbon, strontium, osmium, calcium, neodymium, lithium,  $\text{TEX}_{86}$  and phosphorus; Arthur et al., 1987;

McArthur et al., 2004; Forster et al., 2007; Mort et al., 2007; MacLeod et al., 2008; Turgeon and Creaser, 2008; Voigt et al., 2008; Blättler et al., 2011; Pogge von Strandmann et al., 2013; Zheng et al., 2013) to determine the driving mechanisms for organic carbon burial and anoxia. Among the processes thought to play a role are: enhanced volcanism and  $\text{CO}_2$  output; increased land and sea surface temperatures; an accelerated hydrological cycle, sea level rise and increased rates of ocean circulation; and changes in nutrient supply and productivity. These have all been supported by different proxy studies (e.g. Jenkyns, 1980; Arthur et al., 1987; Arthur and Sageman, 1994; Mort et al., 2007; Turgeon and Creaser, 2008; Martin et al., 2012).

In this study, we present a high-resolution initial osmium isotope ( $^{187}\text{Os}/^{188}\text{Os}$ ;  $\text{Os}_i$ ) stratigraphy of the upper Cenomanian to lower Turonian from 4 transcontinental sections, and the  $\text{Os}_i$  data from two previously analyzed representative sections of the proto-North Atlantic and Tethyan margin (Fig. 1; ODP Site 1260 and Furlo; Turgeon and Creaser, 2008) with additional analysis to enhance resolution. These data are predominantly controlled by

\* Corresponding author. Tel.: +44 0 191 334 2294.

E-mail addresses: [alice.du-vivier@durham.ac.uk](mailto:alice.du-vivier@durham.ac.uk) (A.D.C. Du Vivier), [david.selby@durham.ac.uk](mailto:david.selby@durham.ac.uk) (D. Selby), [brad@earth.northwestern.edu](mailto:brad@earth.northwestern.edu) (B.B. Sageman), [I.Jarvis@kingston.ac.uk](mailto:I.Jarvis@kingston.ac.uk) (I. Jarvis), [d.r.grocke@durham.ac.uk](mailto:d.r.grocke@durham.ac.uk) (D.R. Gröcke), [s.voigt@em.uni-frankfurt.de](mailto:s.voigt@em.uni-frankfurt.de) (S. Voigt).

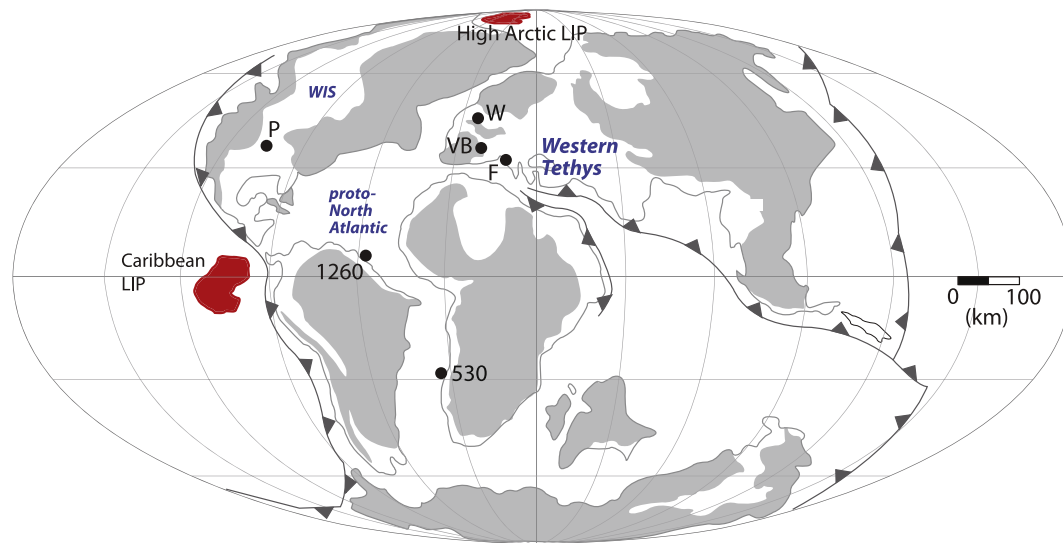


**Fig. 1.** Palaeogeographic map of the CTB showing locations of analyzed sites. P – Portland and Pueblo GSSP; 1260 – ODP Site 1260, Demerara Rise; W – Wunstorf; VB – Vocontian Basin; F – Furlo; 530 – DSDP Site 530. The location of the Caribbean LIP and High Arctic LIP (Large Igneous Province) are also shown.

the mass balance of two end-member Os isotope components: weathered continental crust ( $\sim 1.4$ ) and mantle inputs (0.13) attributed to enhanced submarine volcanism (Peucker-Ehrenbrink and Ravizza, 2000). This, coupled with the short residence time of Os in seawater ( $\leq 10$  kyr; Oxburgh, 2001), makes  $^{187}\text{Os}/^{188}\text{Os}$  composition an excellent monitor of palaeoceanographic changes in the geological record (Peucker-Ehrenbrink and Ravizza, 2000; Cohen, 2004), particularly across the CTB where there is evidence for accelerated weathering, as well as evidence of submarine volcanic activity (Snow et al., 2005; Frijia and Parente, 2008; Turgeon and Creaser, 2008; Pogge von Strandmann et al., 2013).

Analysis of osmium isotope trends recorded from different sites provides information about changes in these inputs to the marine realm, as well as the interconnectivity of oceanic water masses with epeiric seas. The  $\text{Os}_i$  data reported from the previous study show similar profiles, and suggest that for at least  $\sim 700$  kyr of the late Cenomanian–early Turonian the ocean basins were relatively well connected. The  $\text{Os}_i$  data also show that a major pulse of volcanism interpreted to be associated with activity from Large Igneous Provinces (LIPs), i.e., Caribbean and High Arctic (Fig. 1; Snow et al., 2005; Tegner et al., 2011) occurred at or just prior to the onset of OAE 2. However, the High Arctic LIP is largely understudied due to lack of exposure. Since constraints on timing and duration of activity from LIP volcanism are ambiguous (Tegner et al., 2011; Zheng et al., 2013), we associate the  $\text{Os}_i$  data presented here with activity from the better temporally constrained Caribbean LIP (Turgeon and Creaser, 2008).

The  $\text{Os}_i$  stratigraphic profiles across the CTB in this study are from (Fig. 1): the Portland #1 core, which is representative of the Global Stratotype Section and Point (GSSP) near Pueblo, Colorado (Western Interior Seaway (WIS); Kennedy et al., 2000); the Wunstorf core in Germany, a representative section in the NW European pelagic shelf sea (Voigt et al., 2008); the Vocontian Basin, south east France (Western Tethys; Grosheny et al., 2006; Jarvis et al., 2011); and DSDP Site 530 (proto-South Atlantic; Forster et al., 2008). The Portland #1 core has the most refined temporal control for the studied interval based on detailed biostratigraphy, new radioisotopic dating, astrochronology, and chemostratigraphy (Sageman et al., 2006; Meyers et al., 2012a; Ma et al., submitted), and provides a critical framework for global correlation. The Wunstorf core has a similarly good age control based on bio-, chemo-, and cyclostratigraphy and can be correlated to the Portland #1 core succession (Voigt et al., 2008). Based on

the GSSP time scale, and confirmed by additional estimates from different OAE 2 sites, the duration of the C isotope excursion that characterizes the OAE 2 is between 500–600 kyr (Meyers et al., 2012b).

In this study we investigate the  $\text{Os}_i$  stratigraphy of multiple sections over an interval of  $\sim 1.8$  Myr from the late Cenomanian to the early Turonian and demonstrate that  $\text{Os}_i$  values show some differences prior to OAE 2 depending on geographic location and depositional setting. These variations are interpreted to reflect differential water mass exchange between epeiric settings and the open ocean modulated by sea-level change, as well as changes in terrigenous weathering rates due to enhanced global warming, which may have also affected nutrient fluxes and primary production levels. These results suggest that epeiric seas, like the WIS or the European shelf sea, may have played an important role in the driving mechanism for OAE 2.

Additionally, we show that in comparison to the pre-OAE 2 interval, the syn-OAE 2  $\text{Os}_i$  values from Site 1260 and Furlo combined with Portland, Wunstorf, the Vocontian Basin and Site 530 are remarkably similar. Coupled with the new geochronology from the WIS (Meyers et al., 2012a) a refined timing for the onset and duration of LIPs and its temporal association with OAE 2 is developed. Furthermore, our interpretation of the  $\text{Os}_i$  profile concurs with the hypothesis of increased ocean circulation based on analysis of neodymium (Nd) isotopes (Martin et al., 2012; Zheng et al., 2013).

## 2. OAE 2 section geology

### 2.1. Portland #1 Core, Colorado, USA

The studied interval was sampled from the USGS Portland #1 core ( $32^\circ 22.6' \text{N}$ ,  $105^\circ 01.3' \text{W}$ ; Dean and Arthur, 1998; Meyers et al., 2001; Fig. 1). This core was taken about 40 km west of the site near Pueblo, CO that was ratified as the GSSP for the CTB (Kennedy et al., 2005), and its stratigraphy has been correlated, essentially bed for bed, to the GSSP section (Sageman et al., 2006). The Pueblo region was ratified as the GSSP site because the boundary interval contains abundant biostratigraphic index taxa, several options for geochronologic calibration, shows no obvious signs of condensation or significant disconformity, and has various stratigraphic markers that can be correlated over tens of thousands of square km (Hattin, 1971; Elder et al., 1994; Kennedy et al., 2005).

Within the Portland core, the Cenomanian–Turonian Boundary Interval (CTBI) was studied in a 17.7 m-thick section of the Bridge Creek Limestone (~12 m) and Hartland Shale (~12.6 m) Members of the Greenhorn Formation (Cobban and Scott, 1972). These units include organic-rich calcareous shales and rhythmically interbedded couplets of shale and fossiliferous biomicritic limestone. The stratigraphy is also characterized by four bentonite units of 1 to 20 cm that have been regionally correlated (Elder, 1988). Recent sanidine  $^{40}\text{Ar}/^{39}\text{Ar}$  and zircon  $^{206}\text{Pb}/^{238}\text{U}$  geochronology integrated with astrochronology constrain the CTB at  $93.90 \pm 0.15$  Ma (Meyers et al., 2012a). The CTBI contains a variety of fossil taxa useful for biostratigraphy (e.g., Gale et al., 1993; Kennedy et al., 2000, 2005; Keller and Pardo, 2004; Keller et al., 2004; Cobban et al., 2006) some of which have intercontinental distributions; however, their transcontinental synchronicity is limited. The dominant foraminifera species spanning the CTBI are *Rotalipora cushmani*, *Whiteinella archaeocretacea* and *Helvetoglobotruncana helvetica* (Eicher and Worstell, 1970). The FO (first occurrence) of the ammonite *Watinoceras devonense* (Fig. 2; Kennedy et al., 2000) marks the basal Turonian, recorded at the base of bed 86 of the Bridge Creek Limestone (Meyers et al., 2001; bed numbers are based on Cobban and Scott, 1972). The FO of *W. devonense* coincides with the FO of *Mytiloides puebloensis* (Kennedy et al., 2000), which can be traced through both Tethyan and Boreal regions (Kennedy et al., 2005).

The onset of OAE 2 is identified by an abrupt 2–3‰ VPDB  $\delta^{13}\text{C}_{\text{org}}$  positive shift from values of  $\sim -27$ ‰ in the upper Hartland Shale, 4.3 m below the CTB (Fig. 2; Supplementary Material, Table 1a; Sageman et al., 2006). The positive excursion is characteristic of the isotopic response during OAE 2 and, although many localities record increased organic carbon deposition at this level (e.g., Tsikos et al., 2004), sites within the WIS do not. Here the onset is characterized by organic-poor interbedded limestones and shales that are generally bioturbated. Shale interbeds in the upper half of the OAE 2 interval, however, do become enriched in TOC in the WIS. The end of OAE 2 is expressed by a gradual fall in  $\delta^{13}\text{C}_{\text{org}}$  back to  $\sim -27$ ‰ (Sageman et al., 2006).

A high-resolution time scale for the study interval has been developed in recent years based on integration of new radioisotopic dates and astrochronological methods (Meyers et al. 2001, 2012a; Sageman et al., 2006; Ma et al., submitted). The astrochronological techniques yield a more accurate interpolation of time for the intervals between dated tuff horizons because they include evolutive assessment of changes in linear sedimentation rate (not corrected for compaction). Both radioisotopic and astrochronologic methods indicate a duration for OAE 2 of  $\sim 600$  kyr measured from the  $\delta^{13}\text{C}_{\text{org}}$  onset.

## 2.2. Wunstorf, NW Germany

The Wunstorf section was sampled from drill core from  $52^{\circ}24.187'\text{N}$ ,  $09^{\circ}29.398'\text{E}$  and represents the European type section for the CTBI (Fig. 1; Voigt et al., 2008). The CTBI succession (Hesseltal Formation) at Wunstorf was deposited in the distal Lower Saxony Basin, which was part of the western European shelf sea (Wilmsen, 2003). The 26.5 m-thick Hesseltal Formation comprises cyclically interbedded couplets of organic-carbon rich shales, marls and limestones interpreted to represent nine short eccentricity cycles based on spectral analytical results (Voigt et al., 2008). Accordingly, OAE 2, as defined by the  $\delta^{13}\text{C}_{\text{carb}}$  curve, includes 4.3 short eccentricity cycles or 21.2 precession cycles, respectively, indicating a duration of 430–445 kyr (Voigt et al., 2008).

The biostratigraphy of the Hesseltal Formation is established by zonation with inoceramids, ammonites, acme occurrences of macrofossils and planktonic foraminifera (Ernst et al., 1984; Lehmann, 1999; Voigt et al., 2008). The ammonite and inoceramid

zonation can be compared to that of the GSSP in detail. Although no macrofossils are recorded directly from the Wunstorf core, a series of index taxa can be placed based on a bed-by-bed correlation between the Lower Saxony Basin and the Munsterland Cretaceous Basin (Voigt et al., 2007, 2008). The FO of the ammonite *Metaioceras geslinianum* is equivalent to the FO of *Sciponoceras gracile* at the GSSP (Gale et al., 2005, 2008), which corresponds to the base of the Hesseltal Formation at Wunstorf (Lehmann, 1999). The FO of *W. devonense*, the index taxon for the CTB (Fig. 2; Kennedy et al., 2005), is located in the Wunstorf core at  $37.5 \pm 1$  m (Lehmann, 1999; Voigt et al., 2008).

Previously, the stratigraphic extent of OAE 2 was constrained by  $\delta^{13}\text{C}_{\text{carb}}$  (Voigt et al., 2008). Here we present  $\delta^{13}\text{C}_{\text{org}}$  for the Wunstorf section, which shows frequent oscillations from  $-25$  to  $-27$ ‰ VPDB prior to OAE 2 (Fig. 2; Supplementary Material, Table 1b). A facies change depicts the onset throughout the European shelf (Voigt et al., 2007). This change records an initial positive excursion in the  $\delta^{13}\text{C}_{\text{org}}$ , consistent with the  $\delta^{13}\text{C}_{\text{carb}}$ , followed by a second more distinct increase in the  $\delta^{13}\text{C}_{\text{org}}$ . At Wunstorf,  $\delta^{13}\text{C}_{\text{org}}$  only clearly records the second increase; however OAE 2 initiation corresponds to the first increase. The duration of OAE 2 at Wunstorf was estimated to be  $\sim 435$  kyr based on spectral analysis of lithological cyclicity (Voigt et al., 2008), which differs from the astrochronological and radioisotopic derived duration at the GSSP ( $\sim 600$  kyr; applied in this study). Voigt et al. (2008) discussed several options for this discrepancy as the possible lack of strata, different definitions of onset and termination of OAE 2 in the Portland #1 and Wunstorf cores, and incorrect orbital frequency assignment to the dominant cycle length. The new organic  $\delta^{13}\text{C}_{\text{org}}$  curve of this study (Fig. 2) shows five distinct cycles close to the short eccentricity filter of Voigt et al. (2008). Such a reinterpretation would reduce the temporal discrepancy and is consistent with the recently documented stronger obliquity control during OAE 2 (Meyers et al., 2012). Further spectral analytical research is needed to fully address this question.

## 2.3. Vocontian Basin (Pont d'Issole and Vergons), SE France

The Vocontian Basin was part of the western gulf in the European Alpine region of the NW Tethys Ocean  $\sim 30^{\circ}\text{N}$  (Jarvis et al., 2011; Fig. 1). High rates of subsidence throughout the mid-Cretaceous provided accommodation space for thick rhythmically bedded bioturbated limestone–marl successions, where the variable facies are indicative of a fluctuating hemipelagic depositional environment of moderate depth. Different depositional and structural processes dependent on their location in the basin have affected CTB sections within the Vocontian Basin; e.g. the Vergons section is affected by syn-sedimentary slumping in the uppermost Cenomanian, but otherwise exposes a continuous Upper Albian–Lower Turonian succession, while the thinner Pont d'Issole section is complete through the CTBI. A  $\sim 20$  m thick package of black organic-rich calcareous shales, termed the “Niveau Thomeil” (Takashima et al., 2009; Jarvis et al., 2011), characterize the CTBI. Detailed biostratigraphy has been obtained for the 24 m Pont d'Issole section (Groshegy et al., 2006; Jarvis et al., 2011). The distribution of index taxa *R. cushmani* and *H. helvetica*, coupled with complete  $\delta^{13}\text{C}_{\text{org}}$  and  $\delta^{13}\text{C}_{\text{carb}}$  records (Fig. 2; Jarvis et al., 2011), permits bed-scale correlation with the GSSP near Pueblo. Above the onset of OAE 2, samples were taken from Pont d'Issole, whereas below the onset some of the samples ( $n = 4$ ) came from Vergons (Supplementary Material, Table 2d), which is correlated with Pont d'Issole based on litho-, bio-, and stable-isotope stratigraphy and is undisturbed by faulting in the pre-OAE 2 interval.

The OAE 2 in the Pont d'Issole section includes a distinct facies change to finely laminated black shales (total organic carbon, TOC 0.3–3.5 wt.%) that occurs about a metre below the distinctive

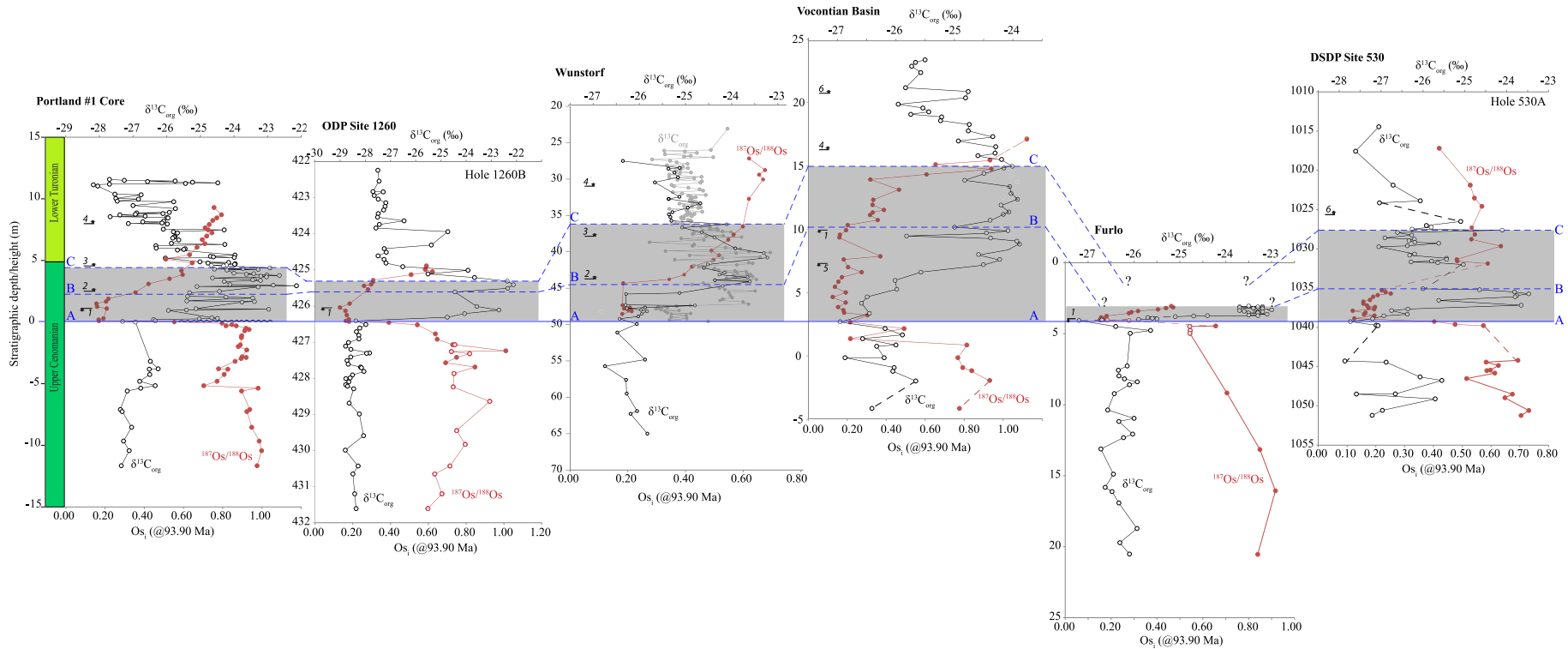


**Fig. 2.**  $\delta^{13}\text{C}_{\text{org}}$  (black) and  $\text{Os}_1$  (red) vs. stratigraphic height/depth. Initial  $^{187}\text{Os}/^{188}\text{Os}$  calculated at 93.90 Ma.  $\delta^{13}\text{C}_{\text{org}}$  data from: Portland #1 Core, Sageman et al. (2006); Site 1260, Forster et al. (2007); Wunstorf (this study); Vocontian Basin, Jarvis et al. (2011); Furlo, Jenkyns et al. (2007); Site 530, Forster et al. (2008). Sites correlated using datum levels on the carbon isotope profiles (A, B, C; see text for details); where 'A' is the positive  $\delta^{13}\text{C}_{\text{org}}$  excursion marks the onset of the OAE 2 (Pratt et al., 1985), 'B' is the trough of relatively depleted values following the initial positive excursion in  $\delta^{13}\text{C}_{\text{org}}$ , and 'C' is the last relatively enriched  $\delta^{13}\text{C}_{\text{org}}$  value before the trend back to pre-excursion values (Tsikos et al., 2004). The positioning of the datum levels is determined for each site based on: Sageman et al., 2006 (Portland #1 Core); Forster et al., 2007 (Site 1260); this study (Wunstorf); Jarvis et al., 2011 (Vocontian Basin); Jenkyns et al., 2007 (Furlo); Forster et al., 2008 (Site 530). Biostratigraphic horizons are labelled: FO – first occurrence, LO – last occurrence; 1 – LO *R. cushmani*; 2 – FO *N. juddii*; 3 – FO *W. devonense*; 4 – FO *H. Helvetica*; 5 – LO *T. greenhornensis*; 6 – FO *Q. gartneri*. The biozones illustrate low resolution and inconsistent global distribution, which restricts correlation. Dashed red lines represent intervals of pore core recovery. Note that symbol size is greater than the measured uncertainty. Carbon and osmium isotope data are reported in Tables 1 and 2 in the Supplementary Material.

positive  $\delta^{13}\text{C}_{\text{org}}$  excursion (3‰) that marks the base of OAE 2 (Fig. 2; Supplementary Material, Table 1d; Jarvis et al., 2011). High-frequency fluctuations in the  $\delta^{13}\text{C}_{\text{org}}$  record, up to 1‰ in magnitude, occur throughout OAE 2, associated with the alternation of lithological units. The termination of OAE 2 is recorded by a gradual return to  $\sim -26\%$ .

#### 2.4. DSDP Site 530, Hole 530A, South Atlantic

Palaeotectonic reconstruction situates Site 530 at 37°S, 38°W (Forster et al., 2008; Fig. 1). Site 530 is located on the abyssal floor of the Angola Basin, 4645 metres below sea level (mbsl) and approximately 150 km west of the base of the continental slope of SW Africa with a 3–4 degree incline. Drilling penetrated to a final depth of 1121 metres below sea floor (mbsf) after encountering durable basalt at 1103 mbsf (Forster et al., 2008). The  $\delta^{13}\text{C}_{\text{org}}$  excursion marking OAE 2 occurs within a 49 m section of the CTBI. Low sample resolution due to poor core recovery, and thus limited nannofossil data, only provide an approximate stratigraphic identification of the CTBI.

Lithology in the CTBI includes interbedded shales, clays and mudstones, some of which are pyritiferous. The organic matter in the black shales is of marine origin, but includes a significant fraction of terrigenous material (Forster et al., 2008). The black shales are highly laminated and relatively undisturbed by bioturbation. The  $\delta^{13}\text{C}_{\text{org}}$  record is incomplete due to poor core recovery and low sample yield, but an excursion signifying OAE 2 is recorded: a 0.5‰ VPDB negative shift immediately precedes the 4‰ positive excursion,  $-27.7$  to  $-23.7\%$  (Fig. 2; Supplementary Material, Table 1f; Forster et al., 2008). The characteristic excursion spans  $\sim 2$  m of finely interbedded shales and mudstones. Throughout OAE 2, the  $\delta^{13}\text{C}_{\text{org}}$  values fluctuate between  $\sim -23.5\%$  to  $-27.5\%$ . The maximum enrichment in the  $\delta^{13}\text{C}_{\text{org}}$  is at 1035.75 mbsf,  $\sim 3.52$  m into OAE 2 (Forster et al., 2008).

#### 2.5. ODP Site 1260, Hole 1260B, Demerara Rise and Furlo, Italy

In an effort to augment the understanding of seawater chemistry prior to OAE 2 provided by Turgeon and Creaser (2008), additional samples ( $n = 12$  [ODP] and  $n = 6$  [Furlo]; Fig. 1) were analyzed and the resolution of the  $\text{Os}_i$  profiles was increased.

The facies at Site 1260 include a mixture of terrigenous detritus and carbonates, with high organic contents up to  $\sim 23$  wt.%. The  $\delta^{13}\text{C}_{\text{org}}$  positive excursion reaches a maximum enrichment of  $-22.1\%$  VPDB and the entire excursion is 1.2 m thick (Fig. 2; Supplementary Material, Table 1c; Forster et al., 2007).

In the Furlo section the CTBI lies within the Scaglia Bianca Formation, which includes abundant biosiliceous limestone. The Livello Bonarelli is a 1 m thick condensed interval of millimetre-laminated black shale and brown radiolarian sand that represents the sedimentary expression of part of OAE 2 (Arthur and Premoli Silva, 1982). Up to 20 m beneath the Bonarelli level there are numerous centimetre scale organic-rich shale layers (Jenkyns et al., 2007). The  $\delta^{13}\text{C}_{\text{org}}$  record has a narrow variation in background values prior to OAE 2,  $\sim -25.9$  to  $-26.5\%$ . The characteristic positive excursion in  $\delta^{13}\text{C}_{\text{org}}$  is a 4‰ shift,  $-27.2$  to  $-23.1\%$ , occurring within  $<0.5$  m (Fig. 2; Supplementary Material, Table 1e).

### 3. Methods

#### 3.1. Analytical protocol

In this study we have applied  $\delta^{13}\text{C}_{\text{org}}$  and Re–Os methodologies to determine the geochemical signatures of OAE 2 related strata. We have used published analytical protocols (e.g., Selby and Creaser, 2003; Jarvis et al., 2011), which are described in detail in

**Table 1**

Age of datum A, B and C to calculate the LSR to derive the Integrated timescale.

$\delta^{13}\text{C}_{\text{org}}$ datum levels <sup>a</sup>	Age (Ma) <sup>b</sup>	kyr	
Portland #1 Core, Colorado, USA			
Datum A	94.38	0	
Datum B	94.23	145	
Datum C	93.95	430	
CTB	93.90	480	
End of OAE 2	93.78	600	
Interval A–B		150	
Interval B–C		280	
Interval C–CTB		50	
Interval A–CTB		480	
	Depth (m)	Datum interval	LSR <sup>c</sup>
ODP Site 1260, Hole 1260B, Demerara Rise			
Datum A	426.41		
Datum B	425.61	A to B	0.53
Datum C	425.31	B to C	0.11
Wunstorf, NW Germany			
Datum A	49.6		
Datum B	44.5	A to B	3.40
Datum C	36.2	B to C	2.96
Vocontian Basin, SE France			
Datum A	1.8		
Datum B	10.3	A to B	5.67
Datum C	15.1	B to C	1.71
Furlo, Italy			
Datum A	4.07		
Datum B	<sup>d</sup>		
CTB	3.05	A to CTB	0.21
DSDP Site 530, Hole 530A, South Atlantic			
Datum A	1039.27		
Datum B	1035.08	A to B	2.79
Datum C	1027.62	B to C	2.66

<sup>a</sup> Determined from the  $\delta^{13}\text{C}_{\text{org}}$  Portland #1 Core by Sageman et al. (2006); see Fig. 2.

<sup>b</sup> Derived from geochronology and astrochronology of GSSP section (Meyers et al., 2012a).

<sup>c</sup> Units cm/kyr.

<sup>d</sup> Datum B in Furlo section is undetermined.

the Supplementary Material together with our sampling protocol from core and outcrop.

#### 3.2. OAE 2 correlation

To date, the CTBI has been correlated ‘globally’ using biostratigraphy and carbon isotope chemostratigraphy. Typically, characteristic peaks and troughs in the  $\delta^{13}\text{C}$  record are combined with key bioevents to establish correlation. The six sections presented here (Fig. 2) are correlated according to this method using points ‘A’, ‘B’ and ‘C’ of the  $\delta^{13}\text{C}_{\text{org}}$  curve that are similar to those first defined by Pratt et al. (1985) in the Western Interior and used later by Tsikos et al. (2004). For this correlation method, ‘A’ represents the last value of relatively depleted  $\delta^{13}\text{C}_{\text{org}}$  before the first major shift to positive values (typically  $-24$  to  $-22\%$ ). This shift marks the base of  $\delta^{13}\text{C}_{\text{org}}$  excursion defined as OAE 2 (reference respective of location). ‘B’ defines a trough of depleted values following the initial positive excursion that occurs prior to the second positive shift (Pratt et al., 1985). ‘C’ is the last relatively enriched  $\delta^{13}\text{C}_{\text{org}}$  value before the trend back toward pre-excursion values, or the end of the so-called “plateau” (Tsikos et al., 2004).

In order to establish a common chronostratigraphic framework for comparing  $\text{Os}_i$  data from distant localities, the chemostratigraphic method described above, confirmed by available biostratigraphic data, is used to extend the Pueblo GSSP timescale from the Portland #1 core (Meyers et al., 2012a) to the other sites. The Portland core record has the highest resolution CTB timescale based

on integration of new radioisotope dates (Ar–Ar and U–Pb) and astrochronology (Meyers et al., 2012a), and new work (Ma et al., submitted) has extended this timescale further down section into the Cenomanian. As a result, our new  $Os_i$  data and  $Os_i$  results from a previous study (Turgeon and Creaser, 2008), can be plotted relative to individual timescales created for each section by exporting temporal information from the Portland #1 core (Fig. 3). Timescale development is based on the following steps (see Table 1):

- i. The new geochronology for the CTBI (Meyers et al., 2012a) employs a short eccentricity band pass to more accurately interpolate the age datum levels between dated tuff horizons. Based on this method, the stage boundary is constrained to  $93.90 \pm 0.15$  Ma.
- ii. The ages of the 'A', 'B' and 'C' markers defined by the  $\delta^{13}C_{org}$  record of the Portland core are also precisely determined using this approach (Fig. 2; Table 1).
- iii. Nominal ages for the 'A', 'B', and 'C' markers are exported to the 'A', 'B' and 'C' datum levels of the  $\delta^{13}C_{org}$  curve in the other sections (Fig. 2), allowing calculation of local linear sedimentation rate values between the datum levels (Table 1). A variable sedimentation rate is more realistic over such time frames, i.e.,  $\sim 100$  kyr. In some sections there is a distinct decrease in rate in the B–C interval, which likely reflects condensation related to global sea-level highstand. Thus, the linear sedimentation rate calculated for A–B is applied to develop a timescale below the 'B' datum, and a linear sedimentation rate for B–C is used for the sections above the 'B' datum (Table 1).
- iv. Each timescale is developed using the onset of 'A' as the temporal datum set to 0 kyr (Fig. 3). This creates a coherent global framework using the onset of  $\delta^{13}C_{org}$  excursion as the key datum level.

Although our methodology increases resolution and reduces uncertainty in the time scales for each section, it cannot eliminate uncertainty (e.g., constant sedimentation rates are still assumed for time scale segments). For the purpose of comparing  $\delta^{13}C_{org}$  and  $Os_i$  records between different localities, however, we believe the chronostratigraphic framework is sufficient to recognize differences in the timing of key events.

### 3.3. Initial $^{187}Os/^{188}Os$ ( $Os_i$ )

The  $Os_i$  values in this study were determined from Re–Os data and the  $^{187}Re$  decay constant ( $1.666e^{-11} a^{-1}$ ; Smoliar et al., 1996; Supplementary Material, Table 2a–f) using the CTB age of 93.90 Ma that was determined from astrochronologic interpolation between volcanic ash ages (based on both  $^{40}Ar/^{39}Ar$  and  $^{206}Pb/^{238}U$  determinations; Gradstein et al., 2012; Meyers et al., 2012a). Analytical uncertainty for individual calculated  $Os_i$  is  $\leq 0.01$ . The reproducibility of calculated  $Os_i$ , based on 12 analyses of the USGS rock reference material SDO-1 (Devonian Ohio Shale), was  $\sim 0.04$  (2 SD; Supplementary Material, Table 3). This uncertainty was used to account for the maximum uncertainty in the sample set for the calculated  $Os_i$ . Calculated  $Os_i$  ratios assume closed system behaviour after deposition with respect to both rhenium and osmium. Furthermore, the  $^{187}Os/^{188}Os$  ratios reflect the isotope composition of the local seawater and are unaffected by mineral detritus.

## 4. Results

### 4.1. Re–Os abundance

Across the onset of OAE 2 there is a dramatic shift to very high values in Os isotope concentration. At Portland Os concentration increases by  $\sim 1000$  ppt within  $\sim 10$  cm; at Wunstorf an increase

of  $\sim 1000$  ppt within  $\sim 30$  cm; Site 1260 increases by  $\sim 1000$  ppt in  $< 60$  cm; in the Vocontian Basin there is an increase of  $\sim 3500$  ppt within 50 cm. In both Furlo and Site 530 there are very considerable changes in the Os concentration;  $> 10000$  ppt within 10 cm and 40 cm, respectively. Conversely, Re abundance is relatively constant at each section, therefore the dramatic difference between the Re and Os abundance produce a similar profile in  $^{187}Re/^{188}Os$  to the  $Os_i$  profile, with an abrupt decrease in the  $^{187}Re/^{188}Os$  directly associated with the abrupt increase in Os.

### 4.2. $^{187}Os/^{188}Os$ isotope stratigraphy

The  $Os_i$  profiles for all six sections show a similar trend; highly radiogenic values that suddenly become unradiogenic, before gradually returning to radiogenic values (Figs. 2, 3; all  $Os_i$  data presented in full in Supplementary Material Table 2). At Portland the  $Os_i$  values show some distinct fluctuations prior to the onset of OAE 2 (point 'A' on the  $\delta^{13}C_{org}$  curve). The Os trend from  $\sim 1.0$  to 0.9, briefly return to  $\sim 1.0$ , and then drop abruptly to  $\sim 0.7$  at  $\sim -237$  kyr (below 'A'). The trend toward unradiogenic values then reverses back toward the radiogenic end member up until the major shift to unradiogenic  $Os_i$  at 'A'.

In the Site 1260 record, a trend from  $\sim 0.6$  to 1.0 in the lowest samples is followed by a shift in the opposite direction, toward the unradiogenic end-member, but the values are variable and some spikes to  $> 1$  (radiogenic) persist. From  $-157$  kyr there is a consistent trend toward unradiogenic  $Os_i$  reaching a minimum value of  $\sim 0.2$  at the 'A' datum. At Wunstorf the rock units prior to 'A' are bereft of Re and Os. The Vocontian Basin records shifts to radiogenic  $Os_i$  values ( $> 0.9$ ), before a gradual decrease to  $\sim 0.76$  followed by a brief increase to  $\sim 0.82$ . A few metres below the positive excursion a major shift to  $< 0.3$  occurs. The  $Os_i$  values at Furlo remain stable at  $\sim 0.55$  then shift suddenly to  $\sim 0.65$ . Above this horizon there are no samples until 'A' when the  $Os_i$  is unradiogenic  $< 0.3$ . Site 530 has  $Os_i$  values of  $\sim 0.70$  before showing a 0.2 decrease. The trend reverses to  $\sim 0.7$ , then the major unradiogenic shift to  $< 0.2$  at 'A'. Importantly, the  $Os_i$  record in the Portland core (Fig. 3) is significantly different between  $\sim -230$  kyr and  $\sim -50$  kyr relative to the other 4 sites (no data for Wunstorf).

From 'A' through to the lower Turonian, the  $Os_i$  profiles and values are very similar across Portland, Furlo, Site 530 and Wunstorf, progressively trending from unradiogenic ( $\sim 0.2$ ) to radiogenic values ( $\sim 0.6$  to 0.7; Fig. 3) within  $\sim 350$  kyr. The  $Os_i$  values from point 'A' remain unradiogenic for  $\sim 200$ – $250$  kyr before becoming progressively more radiogenic (Fig. 3). The majority of the  $Os_i$  data from the Vocontian Basin, from slightly before the onset of the positive  $\delta^{13}C_{org}$  excursion through the initial  $\sim 200$  kyr are unradiogenic at  $\sim 0.2$ , with some fluctuation to  $\sim 0.4$ . In contrast to other sites that show a progressive return to radiogenic  $Os_i$  values, the Vocontian Basin remains at values of  $\sim 0.4$  for an additional 200 kyr and then becomes radiogenic (0.94) very rapidly (within  $\sim 80$  kyr; Fig. 3). This abrupt change could indicate a minor hiatus during the latter part of OAE 2. The  $Os_i$  values at Site 530 remain unradiogenic (0.12–0.25) for  $\sim 145$  kyr, returning to radiogenic values after  $\sim 270$  kyr. However, due to poor core recovery there is a  $\sim 125$  kyr gap in the  $Os_i$  record (Fig. 3).

## 5. Discussion

### 5.1. Heterogeneous seawater $^{187}Os/^{188}Os$ prior to OAE 2

Overall the  $Os_i$  profiles from each section show similar variability in  $Os_i$  values and in the  $^{187}Re/^{188}Os$  composition before and during OAE 2. Combined with previous Os isotope stratigraphy (Turgeon and Creaser, 2008) and detailed litho-, bio-, and

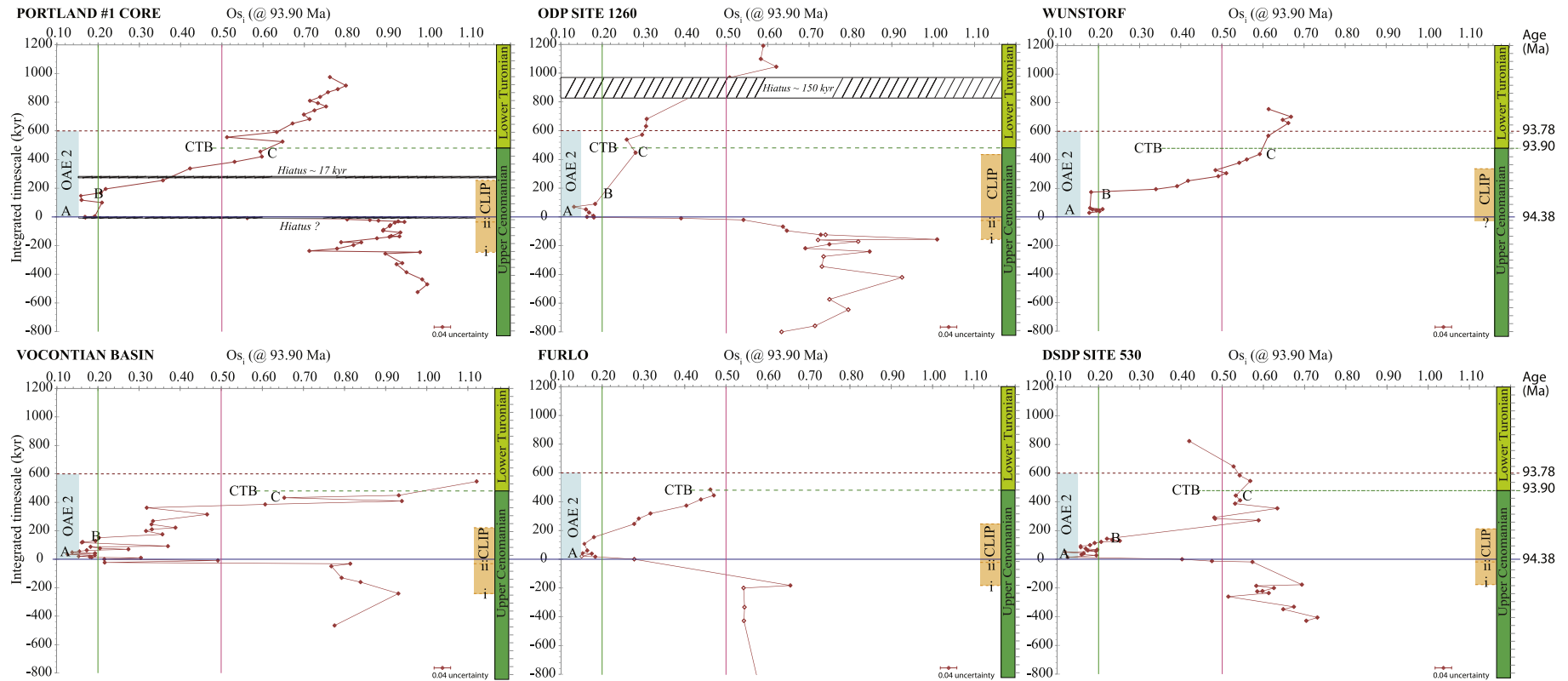


**Fig. 3.**  $Os_i$  data calculated at 93.90 Ma relative to chemostratigraphically integrated timescales (kyr). 0 kyr marks the onset of OAE 2 (~94.38 Ma) that is equal to the onset of the positive  $\delta^{13}C_{org}$  excursion and defined as datum 'A'. The  $\delta^{13}C_{org}$  profile also includes markers 'B' and 'C'. These datum levels provide the basis for chemostratigraphic correlation within the OAE 2 interval. The green dashed line shows the CTB. The blue shaded area from 0 to 600 kyr illustrates the duration of OAE 2 (Sageman et al., 2006), and the red dashed line represents the upper limit of the event. The initial onset of CLIP volcanism 'i' is at ~94.58 Ma, with the major pulse 'ii' at ~94.41 Ma and main cessation at ~94.13 Ma (CLIP – Caribbean LIP). Uncertainty on all ages is nominally  $\pm 0.2$  Ma (Meyers et al., 2012a). The open red squares are the additional samples analyzed for Site 1260B and Furlo in this study, the remainder of the data for these localities are from Turgeon and Creaser (2008). The grey hatched sections represent hiatuses: Portland hiatus just prior to the onset of OAE 2 is minor and has an un-quantified duration (Ma et al., submitted). The hiatus at Site 1260 is based on core images and the  $\delta^{13}C_{org}$  profile (this study, see Section 5.3. for discussion). Vertical lines at  $Os_i$  values 0.2 and 0.5 facilitate comparison of absolute values between profiles;  $Os_i$  values <0.2 represent a predominantly hydrothermal source, >0.5 represent a predominance of continental weathering. Note that individual  $Os_i$  uncertainty is <0.01 and thus symbol size is greater than the measured uncertainty. Uncertainty is shown based on 2SD of 12 analyses of SDO-1 is <0.04.

chemostratigraphy, the sections are interpreted to be reliable records of the CTBI.

The  $\text{Os}_i$  values for all sites in the WIS, western Tethys and proto-North Atlantic from  $-800$  kyr to  $-210$  kyr are radiogenic, and range from  $\sim 0.5$  to  $\sim 1.0$ , illustrating that the seawater  $^{187}\text{Os}/^{188}\text{Os}$  ratio during this time was not homogeneous, but was controlled by the  $^{187}\text{Os}/^{188}\text{Os}$  composition of the fluxes entering the individual basins (Figs. 1, 3). The radiogenic heterogeneity and high  $\text{Os}_i$  values at Portland are attributed to the influence of weathered crustal components from the Sevier Orogenic Belt and the Canadian Shield, the major sources of weathered material to the basin. Recent seawater Os isotope studies during glacial episodes in the last 200 kyr demonstrate how regional variation is correlated to the heterogeneous flux of material into proximal basins (Paquay and Ravizza, 2012). This hypothesis is supported by the observed radiogenic  $\text{Os}_i$  values for  $>500$  kyr prior to 'A' at Portland and elsewhere (Fig. 3). We therefore infer that water masses were reasonably well connected until  $\sim -210$  kyr, but the  $^{187}\text{Os}/^{188}\text{Os}$  composition of the seawater in the individual basins was strongly influenced by regional factors (Figs. 1, 3). In addition, the heterogeneity of the  $^{187}\text{Os}/^{188}\text{Os}$  data may provide information on vertical mixing as a function of depth and circulation; the variations may indicate that seawater was not always well mixed.

#### 5.1.1. Implications of basin connectivity

Between  $\sim -300$  and  $-200$  kyr,  $\text{Os}_i$  values at Portland in the WIS reverse toward more radiogenic values. A similar pattern is observed at Site 1260, Vocontian Basin, Furlo and Site 530, although in each of these sites the radiogenic  $\text{Os}_i$  inflection is brief (only a single data point) before the decline in  $\text{Os}_i$  values (Fig. 3). There are two possible mechanisms that could contribute to produce an  $\text{Os}_i$  signal of this type within a shallow epeiric seaway: increased input of weathered material and restriction of the connection to the open ocean, which would allow a radiogenic (weathering input) signal to dominate (e.g., Portland and the Vocontian Basin). In contrast, it is assumed that deep water sites preserve a signal more consistently representative of the open ocean (e.g., Site 1260 and 530).

The shallow epeiric setting at Portland would certainly have become restricted from the global ocean during sea-level lowstands, however, the degree of sea level fall necessary to produce restriction is difficult to know. There is evidence of a small hiatus and a bone bed within the uppermost Hartland Shale, and two seaward stepping parasequences in the Dakota Formation of SW Utah correlate basinward to a level just below this hiatus (Elder et al., 1994), suggesting that a minor relative sea-level fall may have occurred (Gale et al., 2008). Subsequently, the lowermost beds of the Bridge Creek Limestone contain a diverse marine fauna with many Tethyan taxa (Kauffman, 1984), and there is strong evidence for transgression during the deposition of the basal limestone bed (Arthur and Sageman, 2005). Thus, the onset may have been immediately preceded by a relative fall in sea level that could have briefly reduced or shut down exchange of water masses with the global ocean, followed by a rapid sea-level rise.

Basin restriction may also provide an explanation for the delayed return to pre-OAE 2  $\text{Os}_i$  values in the Vocontian Basin.  $\text{Os}_i$  values return to  $\sim 0.3$  at 'B' comparable to other sections (Fig. 3). Yet between 'B' and 'C' the  $\text{Os}_i$  values fluctuate around  $\sim 0.4$  for an additional  $\sim 200$  kyr relative to other sites, which suggests that mixing with the rest of the proto-North Atlantic was temporarily limited.

#### 5.1.2. Implications of enhanced weathering

To explain the radiogenic pre-OAE 2  $\text{Os}_i$  values, a continuous radiogenic continental input into the ocean is required (Peucker-Ehrenbrink and Ravizza, 2000). Hence, the other mech-

anism resulting in radiogenic  $\text{Os}_i$  values is a significant increase in the flux of weathered material to a basin. Interpreted increases in temperature before 'A' indicate a period of significant warming (Clarke and Jenkyns, 1999; Forster et al., 2007; Jenkyns et al., 2004; Barclay et al., 2010), an intensification of the hydrological cycle, and more extensive flooding in continental interiors, which led to the build-up of terrestrially derived nutrients and organic-rich sediments in shallow basin water masses immediately prior to 'A'. The radiogenic  $\text{Os}_i$  prior to 'A' reflects sequestration of hydrogenous Os derived from the continent as a result of high weathering rates. If, in fact, the WIS did become briefly restricted, the influence of local weathering inputs and changes in mixing between basins would be amplified in the seawater chemistry.

Additionally, there is evidence that increased input of weathered material influenced the Os chemistry of the shallow bathyal Site 1260 and the abyssal Site 530 before 'A'. Continental turbiditic sediments deposited on the continental slope at Site 1260 produce an oscillating  $\text{Os}_i$  profile before the onset. At Site 530, comparatively less radiogenic  $\text{Os}_i$  values prior to 'A' suggest that juvenile turbidites were sourced from juvenile detritus from the Walvis Ridge.

The high rates of weathering produced waters enriched in micro-nutrients that led to an increase in productivity coincident with OAE 2, which is supported by bulk rock enrichments of Si, P, Ba, Cu, Mo, Ni and Zn in black shales at Demerara Rise ODP sites (Jimenez Berrosoco et al., 2008). In addition, enhanced weathering is inferred from Sr isotope trends, which despite possessing a longer residence time (1–4 Ma) have been interpreted to reflect global warming prior to, and during OAE 2 (Frijia and Parente, 2008).

#### 5.2. Caribbean large igneous province and OAE 2

In contrast to the elevated radiogenic  $\text{Os}_i$  values just before 'A' at Portland, the  $\text{Os}_i$  values of Site 1260, Vocontian Basin, Furlo and Site 530 show a progressive trend to unradiogenic  $\text{Os}_i$  values (0.75 to 0.55) over  $\sim 155$  kyr (Fig. 3) suggesting that hydrothermal input dominated Os chemistry in the open oceans. Within the WIS the stratigraphic evidence for sea-level rise is coincident with an abrupt shift of radiogenic  $\text{Os}_i$  values to very unradiogenic values at Portland  $\sim 50$  kyr prior to 'A'. Therefore the trend to almost homogeneous unradiogenic  $\text{Os}_i$  recorded in all sites at 'A' requires a sustained source of unradiogenic Os input to the ocean.

Basaltic igneous provinces release unradiogenic Os, close to chondritic values ( $\sim 0.13$ ; Cohen and Coe, 2002). There are two potential sources of volcanism: the Caribbean LIP and the High Arctic LIP. The eruption history from the High Arctic remains poorly constrained (Tegner et al., 2011) and trends interpreted at this stage are relatively ambiguous (Zheng et al., 2013). Consequently, the abrupt unradiogenic trend is interpreted to reflect an episode of submarine mafic volcanism from the Caribbean LIP (Fig. 3), sufficient to influence the global Os isotope budget (Turgeon and Creaser, 2008).

The high-resolution of the  $\text{Os}_i$  data presented here make an important contribution to the discussion of Caribbean LIP onset and cessation. Evidence supports the hypothesis that an influx of unradiogenic Os in the marine Os record is a direct consequence of volcanism (Ravizza and Peucker-Ehrenbrink, 2003). From  $\sim -50$  kyr all sites show a synchronous abrupt trend towards unradiogenic  $\text{Os}_i$  values (Fig. 3). Based on the trend to unradiogenic  $\text{Os}_i$  values at Site 1260, Vocontian Basin, Furlo and Site 530 we suggest that the initiation of volcanism was at least  $\sim 200$  kyr prior to 'A' ( $\sim 94.58$  Ma; Fig. 3, CLIP i), with the major pulse of submarine volcanism happening at  $\sim -30$  kyr (94.41 Ma; Fig. 3, CLIP ii), where all locations possess near mantle-like  $\text{Os}_i$  values. The timing of Caribbean LIP ii is supported by the rapid change in Os



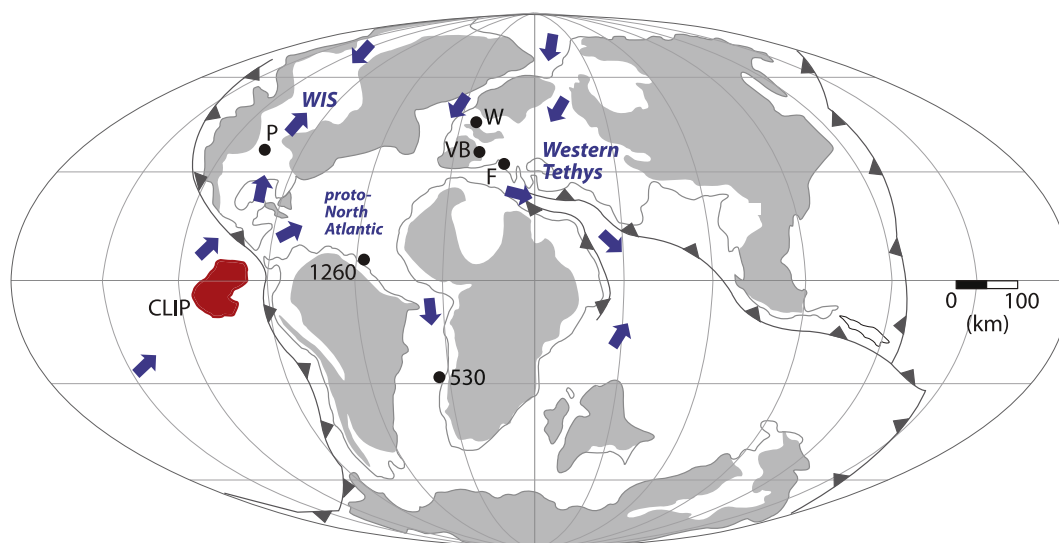


**Fig. 4.** Palaeocirculation pattern during the Cenomanian–Turonian boundary interval. Blue arrows represent the direction of palaeocirculation interpreted based on this study, Slingerland et al. (1996) and Trabucho-Alexandre et al. (2010).

concentration (Section 4.2; Supplementary Material, Table 2) in all sections with the exception of Wunstorf where there is no record (Fig. 3). The sudden and high increase in Os concentrations occurs within 1 metre of deposition, which equates to <20 kyr at Furlo and Site 530, and <10 kyr at Portland, Site 1260 and Vocontian Basin. The increase in concentration is directly synchronous with the abrupt decrease to very low seawater  $Os_i$  values and is contemporaneous with 'A' within <20 kyr.

The trend recorded in the new sections studied here is consistent with the pattern observed in the previous work by Turgeon and Creaser (2008), where there was a clear and large increase in Os concentration at the onset of OAE 2. As discussed, high weathering rates across the CTB released large amounts of organic-rich material to the oceans, which sequester hydrogenous Os (Peucker-Ehrenbrink and Ravizza, 2000). The trend therefore implies that within <20 kyr the amount of unradiogenic dissolved Os to seawater significantly reduced the influence of radiogenic Os (Cohen and Coe 2002, 2007; Ravizza and Peucker-Ehrenbrink, 2003). Therefore, the observed regional variations in the data support the short residence time of Os in seawater and confirm the capability of Os to detect short-term forcing mechanisms, such as activity from LIPs.

The interaction of both volcanism and enhanced global weathering on  $Os_i$  means that quantifying the magnitude and isolating the extent of the two signals is problematic, since the extent of weathering on seawater chemistry is masked by the inputs from the Caribbean LIP to the global ocean. We can only estimate the Os contribution to seawater chemistry using a mixing model and assumed abundances. If we assume that the average seawater  $^{187}Os/^{188}Os$  prior to the LIP onset was  $\sim 0.8$ , and use an average Os abundance in seawater of 10 ppq (based on the present-day average; Peucker-Ehrenbrink and Ravizza, 2000), a basalt  $^{187}Os/^{188}Os$  of 0.13 (Meisel et al., 2001) and an average Os abundance, we can evaluate the approximate Os contribution from the Caribbean LIP to the global ocean using a progressive mixing model (Faure, 1986, Eqs. (9.2) and (9.10)). We note that there are no published Os data for the Caribbean LIP. However, basalts can have variable Os abundances (1 to 600 ppt; Martin, 1991; Crocket and Paul, 2008); typical values range from 1 to 30 ppt (e.g., Shirey and Walker, 1998; Allegre et al., 1999; Dale et al., 2008). Using an Os abundance for a basalt of 30 ppt would require 75% Os contribution from the LIP to yield the least radiogenic  $Os_i$  observed at all locations. Considerably less Os input from the LIP (25%) is needed if the LIP basalts

possess higher Os abundances (100 ppt) and if the Os contribution to seawater also occurred through the addition of gas known to be enriched 20 times that of the basalt (e.g., Yudovskaya et al., 2008).

If we assume the emplacement and weathering of the LIP are direct indicators of volcanic activity (Cohen and Coe 2002, 2007), we can estimate the duration of volcanism at the Caribbean LIP based on the marine  $^{187}Os/^{188}Os$  record. During the emplacement of the LIP we assume that growth of the plateau does not continue to affect the Os isotope composition (Robinson et al., 2009), since the  $Os_i$  values are homogeneous ( $\sim 0.2$ ; Fig. 3). The subsequent trend to radiogenic  $Os_i$  values  $\sim 200$  kyr after 'A' potentially represents the cessation of volcanism. If we consider that the predominant  $^{187}Os/^{188}Os$  of the ocean prior to the Caribbean LIP was 0.8, the influence of Os abundance and isotopic composition from the Caribbean LIP was less than 5% once the seawater  $^{187}Os/^{188}Os$  had reached  $\sim 0.50$ , which occurred  $\sim 450$  kyr after the onset (until  $\sim 94.13$  Ma; Fig. 3).

### 5.3. Hiatuses identified during the CTBI

At Portland the  $\sim 17$  kyr hiatus above 'B' was previously identified by Meyers and Sageman (2004), and the hiatus just before 'A', though quantitatively unconstrained, is equally minor based on site comparison (Elder et al., 1994; Ma et al., submitted). This study has identified one hiatus in the higher part of the OAE 2 at Site 1260. At Site 1260 Erbacher et al. (2005) suggested that  $\sim 150$  kyr is missing from Site 1258, yet present at Site 1260. However, distinct lithological breaks in the core images at 425.19 m and the  $\delta^{13}C_{org}$  record indicate that the hiatus may also be present in the latter section. A 150 kyr hiatus is inferred here from the Os isotope profile (Fig. 3).

### 5.4. Palaeocirculation across OAE 2

A model of quasi-estuarine circulation that was proposed for the WIS, which includes surface outflows causing deeper Atlantic/Tethyan water masses to be advected into the basin (Slingerland et al., 1996), is also suggested as a means to import Caribbean LIP influenced proto-Pacific waters into the proto-Atlantic and Tethys (Trabucho-Alexandre et al., 2010). The similar shape of the  $Os_i$  profiles (from  $\sim -50$  kyr until  $\sim 200$  kyr into OAE 2) suggest that unradiogenic Os-bearing water was rapidly transported from the proto-Pacific into and across the proto-North

Atlantic/Tethys, and into the WIS (Fig. 4). This model is consistent with the hypothesis that palaeocirculation was not sluggish, as also indicated by climate models (Trabucho-Alexandre et al., 2010) and data from Nd isotopes. The latter suggest a dynamic deep/bottom-water circulation (MacLeod et al., 2008; Martin et al., 2012) that is interpreted to reflect the relationship between bottom-water sources, climate, ocean anoxia, and circulation (Martin et al., 2012).

## 6. Conclusions

Submarine volcanism alone cannot be the sole driving mechanism for OAEs, especially OAE 2.  $Os_i$  data from 6 transatlantic and epeiric sections demonstrate that OAE 2 resulted from a combination of interacting factors. An influx of nutrients from the continents preconditioned the oceans and helped to trigger OAE 2 through increased productivity and, similarly to Jones and Jenkyns (2001), we infer that rising sea level may have been the tipping point for the development of widespread anoxia. The  $Os_i$  profile at Portland suggests that the restriction of the epeiric WIS during the pre-OAE 2 interval amplified the effects of high weathering rates as abundant organic-rich sediments sequestered radiogenic Os derived from the ancient continental crust. The close similarity of  $Os_i$  profiles from ~50 kyr prior to the OAE 2 and throughout the syn-OAE 2 interval indicates that transgression progressed to a point where a homogeneous global seawater signal was delivered to multiple proto-transatlantic basins by active ocean circulation. Furthermore, the synchronicity of the unradiogenic  $Os_i$  pattern suggests that the magnitude of Caribbean LIP volcanism was sufficient to simultaneously influence the seawater chemistry of each basin; the abundance of organic-rich sediments added to the water column as a result of enhanced continental weathering permitted sequestration of hydrogenous unradiogenic Os from the contemporaneous Caribbean LIP. The temporal coincidence provides empirical evidence for the duration of the Caribbean LIP of ~450 kyr.

## Acknowledgements

We would like to thank C. Dale, A. Finlay, J. Trabucho-Alexandre, and Joanne Peterkin for laboratory assistance and discussion. Thanks to H.C. Jenkyns for providing additional samples from Furlo for  $Os_i$  analysis. The project was possible thanks to a NERC small grant to D.S. and D.R.G. (NE/G009678/1), NERC standard grants to D.R.G. and D.S. (NE/H021868/1) and I.J. (NE/H020756/1), BP funding to D.S., and a grant for fieldwork awarded to A.D.C. Du Vivier by the Geologists' Association. We are grateful for the constructive reviews from H. Jenkyns, G. Ravizza and G. Henderson that helped improve this manuscript.

## Appendix A. Supplementary material

Supplementary material related to this article can be found online at <http://dx.doi.org/10.1016/j.epsl.2013.12.024>.

## References

- Allegre, C.J., Birck, J.L., Capmas, F., Courtillot, V., 1999. Age of the Deccan traps using  $^{187}\text{Re}$ – $^{187}\text{Os}$  systematic. *Earth Planet. Sci. Lett.* 170, 197–204.
- Arthur, M.A., Premoli Silva, I., 1982. Development of widespread organic carbon-rich strata in the Mediterranean Tethys. In: Schlanger, S.O., Cita, M.B. (Eds.), *Nature and Origin of Cretaceous Carbon-Rich Facies*. Academic, London, pp. 7–54.
- Arthur, M.A., Sageman, B.B., 1994. Marine black shales: Depositional mechanisms and environments of ancient deposits. *Annu. Rev. Earth Planet. Sci.* 22, 499–551.
- Arthur, M.A., Sageman, B.B., 2005. Sea level control on source rock development: Perspectives from the Holocene Black Sea, the mid-Cretaceous Western Interior Basin of North America, and the Late Devonian Appalachian Basin. In: Harris, N.B. (Ed.), *The Deposition of Organic Carbon-Rich Sediments: Models, Mechanisms and Consequences*. In: *SEPM Spec. Publ.*, vol. 82, pp. 35–59.
- Arthur, M.A., Schlanger, S.O., Jenkyns, H.C., 1987. The Cenomanian/Turonian Oceanic Anoxic Event, II: Palaeoceanographic controls on organic matter production and preservation. In: Brooks, J., Fleet, A.J. (Eds.), *Marine Petroleum Source Rocks*. In: *Geol. Soc. (Lond.) Spec. Publ.*, vol. 26, pp. 401–420.
- Barclay, R.S., McElwain, J.C., Sageman, B.B., 2010. Carbon sequestration activated by a volcanic  $\text{CO}_2$  pulse during Oceanic Anoxic Event 2. *Nat. Geosci.* 3. <http://dx.doi.org/10.1038/NGEO757>.
- Blättler, C.L., Jenkyns, H.C., Reynard, L.M., Henderson, G.M., 2011. Significant increases in global weathering during Oceanic Anoxic Events 1a and 2 indicated by calcium isotopes. *Earth Planet. Sci. Lett.* 309, 77–88.
- Clarke, L.J., Jenkyns, H.C., 1999. New oxygen isotope evidence for long-term Cretaceous climatic change in the Southern Hemisphere. *Geology* 27 (8), 699–702.
- Cobban, W.A., Scott, G.R., 1972. *Stratigraphy and ammonite fauna of the Graneros Shale and Greenhorn Limestone near Pueblo, Colorado*. U.S. Govt. Printing Office (Washington), 101–368–424.
- Cobban, W., Walaszczuk, I., Obradovich, J.D., McKinney, K.C., 2006. A USGS zonal table for the Upper Cretaceous Middle Cenomanian–Maastrichtian of the Western Interior of the United States based on ammonites, inoceramids, and radiometric ages. USGS Open-File Report 2006-1250.
- Cohen, A.S., 2004. The rhenium-osmium isotope system: Applications to geochronological and palaeoenvironmental problems. *Mem. Geol. Soc. Lond.* 161, 729–734.
- Cohen, A., Coe, A., 2002. New geochemical evidence for the onset of volcanism in the Central Atlantic magmatic province and the environmental change at the Triassic–Jurassic boundary. *Geology* 30, 267–270.
- Cohen, A., Coe, A., 2007. The impact of the Central Atlantic Magmatic Province on climate and on the Sr- and Os-isotope evolution of seawater. *Palaeogeog. Palaeoclimatol. Palaeoecol.* 244, 374–390.
- Crocket, J.H., Paul, D.K., 2008. Platinum-group elements in igneous rocks of the Kutch rift basin, NW India: Implications for relationships with the Deccan volcanic province. *Chem. Geol.* 248, 239–255.
- Dale, C.W., Luguet, A., Macpherson, C.G., Pearson, D.G., Hickey-Vargas, R., 2008. Extreme platinum-group element fractionation and variable Os isotope compositions in Philippine Sea Plate basalts: Tracing mantle source heterogeneity. *Chem. Geol.* 248, 213–238.
- Dean, W.E., Arthur, M.A., 1998. Geochemical expression of cyclicity in Cretaceous pelagic limestone sequences: Niobrara Formation, Western Interior Seaway. In: Dean, W.E., Arthur, M.A. (Eds.), *Stratigraphy and Palaeoenvironments of the Cretaceous Western Interior Seaway, U.S.A.* In: *Concepts in Sedimentology and Palaeontology*, vol. 6. SEPM, pp. 227–255.
- Eicher, D.L., Worstell, P., 1970. Cenomanian and Turonian foraminifera from the Great Plains, United States. *Micropaleontology* 16, 269–324.
- Elder, W.P., 1988. Geometry of Upper Cretaceous bentonite beds: implications about volcanic source areas and paleowind patterns, western interior, United States. *Geology* 16, 835–838.
- Elder, W.P., Gustason, E.R., Sageman, B.B., 1994. Correlation of basinal carbonate cycles to nearshore parasequences in the Late Cretaceous Greenhorn Seaway, Western Interior, U.S.. *Geol. Soc. Am. Bull.* 106, 892–902.
- Erbacher, J., Friedrich, O., Wilson, P.A., Birch, H., Mutterlose, J., 2005. Stable organic carbon isotope stratigraphy across Oceanic Anoxic Event 2 of Demerara Rise, western tropical Atlantic. *Geochem. Geophys. Geosyst.* 6, Q06010. <http://dx.doi.org/10.1029/2004GC000850>.
- Ernst, G., Wood, C.J., Hilbrecht, H., 1984. The Cenomanian–Turonian boundary problem in NW-Germany with comments on the north–south correlation to the Regensburg area. *Bull. Geol. Soc. Denmark* 33, 103–113.
- Faure, G., 1986. *Principles of Isotope Geology*, 2nd edition. John Wiley & Sons, Inc., ISBN 0-471-86412-9.
- Forster, A., Schouten, S., Moriya, K., Wilson, P.A., Sinninghe Damsté, J.S., 2007. Tropical warming and intermittent cooling during the Cenomanian/Turonian oceanic anoxic event 2: Sea surface temperature records from the equatorial Atlantic. *Palaeoceanography* 22, PA1219. <http://dx.doi.org/10.1029/2006PA001349>.
- Forster, A., Kuypers, M.M.M., Turgeon, S.C., Brumsack, H.-J., Petrizzo, M.R., Sinninghe Damsté, J.S., 2008. The Cenomanian/Turonian oceanic anoxic event in the South Atlantic: New insights from a geochemical study of DSDP 530A. *Palaeogeog. Palaeoclimatol. Palaeoecol.* 267, 256–283.
- Frijia, G., Parente, M., 2008. Strontium isotope stratigraphy in the upper Cenomanian shallow-water carbonates of the southern Apennines: Short-term perturbations of marine  $^{87}\text{Sr}/^{86}\text{Sr}$  during the oceanic anoxic event 2. *Palaeogeog. Palaeoclimatol. Palaeoecol.* 261, 15–29.
- Gale, A.S., Jenkyns, H.C., Kennedy, W.J., Corfield, R.M., 1993. Chemostratigraphy versus biostratigraphy: Data from around the Cenomanian–Turonian boundary. *J. Geol. Soc.* 150, 29–32.
- Gale, A.S., Kennedy, W.J., Voigt, S., Walaszczuk, I., 2005. Stratigraphy of the Upper Cenomanian–Lower Turonian Chalk succession at Eastbourne, Sussex, UK: ammonites, inoceramid bivalves and stable carbon isotopes. *Cretaceous Res.* 26 (3), 460–487.
- Gale, A.S., Voigt, S., Sageman, B.B., Kennedy, W.J., 2008. Eustatic sea-level record for the Cenomanian (Late Cretaceous) – Extension to the Western Interior Basin, USA. *Geology* 36, 859–862.
- Gradstein, F.M., Ogg, J.G., Schmitz, M. (Eds.), 2012. *The Geologic Time Scale 2012*, 2-volume set. Elsevier.

- Grosheny, D., Beaudoin, B., Morel, L., Desmares, D., 2006. High-resolution biostratigraphy and chemostratigraphy of the Cenomanian/Turonian boundary event in the Vocontian Basin, southeast France. *Cretaceous Res.* 27, 629–640.
- Hattin, D.E., 1971. Widespread, synchronously deposited, burrow-mottled limestone beds in Greenhorn Limestone (Upper Cretaceous) of Kansas and central Colorado. *Am. Assoc. Pet. Geol. Bull.* 55, 412–431.
- Jarvis, I., Lignum, J.S., Grocke, D.R., Jenkyns, H.C., Pearce, M.A., 2011. Black shale deposition, atmospheric CO<sub>2</sub> drawdown, and cooling during the Cenomanian–Turonian Oceanic Anoxic Event. *Paleoceanography* 26, PA3201. <http://dx.doi.org/10.1029/2010PA002081>.
- Jenkyns, H.C., 1980. Cretaceous anoxic events: from continents to oceans. *Mem. Geol. Soc. Lond.* 137, 171–188.
- Jenkyns, H.C., Forster, A., Schouten, S., Sinninghe Damste, J.S., 2004. High temperatures in the Late Cretaceous Arctic Ocean. *Nature* 432, 888–892.
- Jenkyns, H.C., Matthews, A., Tsikos, H., Erel, Y., 2007. Nitrate reduction, sulfate reduction, and sedimentary iron isotope evolution during the Cenomanian–Turonian oceanic anoxic event. *Paleoceanography* 22, PA3208. <http://dx.doi.org/10.1029/2006PA001355>.
- Jimenez Berrosoco, A., MacLeod, K.G., Calvert, S.E., Elorza, J., 2008. Bottom water anoxia, inoceramid colonization, and benthopelagic coupling during black shale deposition on Demerara Rise. *Paleoceanography* 23, PA3212. <http://dx.doi.org/10.1029/2007PA001545>.
- Jones, C.E., Jenkyns, H.C., 2001. Seawater strontium isotopes, oceanic anoxic events, and seafloor hydrothermal activity in the Jurassic and Cretaceous. *Am. J. Sci.* 301, 112–149.
- Kauffman, E.G., 1984. Paleobiogeography and evolutionary response dynamic in the Cretaceous Western Interior Seaway of North America. In: Westermann, G.E.G. (Ed.), *Jurassic–Cretaceous Biochronology and Paleogeography of North America*. In: *Geol. Assoc. Canada Spec. Paper*, vol. 27, pp. 273–306.
- Keller, G., Pardo, A., 2004. Age and paleoenvironment of the Cenomanian/Turonian global stratotype section and point at Pueblo, Colorado. *Marine Micropaleontology* 51, 95–128.
- Keller, G., Berner, Z., Adatte, T., Stueben, D., 2004. Cenomanian–Turonian and  $\delta^{13}\text{C}$  and  $\delta^{18}\text{O}$ , sea level and salinity variations at Pueblo, Colorado. *Palaeogeog. Palaeoclimatol. Palaeoecol.* 211, 19–43.
- Kennedy, W.J., Walaszczyk, I., Cobban, W.A., 2000. Pueblo, Colorado, USA, candidate Global Boundary Stratotype Section and Point for the base of the Turonian Stage of the Cretaceous and for the base of the middle Turonian Substage, with a revision of the Inoceramidae (Bivalvia). *Acta Geologica Polonica* 50, 295–334.
- Kennedy, W.J., Walaszczyk, I., Cobban, W.A., 2005. The global boundary stratotype section and point for the base of the Turonian Stage of the Cretaceous: Pueblo, Colorado, USA. *Episodes* 28, 93–104.
- Lehmann, J., 1999. Integrated stratigraphy and palaeoenvironment of the Cenomanian–Lower Turonian (Upper Cretaceous) of Northern Westphalia, North Germany. *Facies* 40, 25–70.
- Ma, C., Meyers, S.R., Sageman, B.B., Singer, B.S., Jicha, B.R., submitted. Testing the astronomical time scale for Oceanic Anoxic Event 2, and its extension into Cenomanian strata of the Western Interior Basin. *Geol. Soc. Am. Bull.* Submitted for publication.
- MacLeod, K.G., Marin, E.E., Blair, S.W., 2008. Nd excursions across the Cretaceous oceanic anoxia event 2 (Cenomanian–Turonian) in the tropical North Atlantic. *Geology* 36, 811–814.
- Martin, C.E., 1991. Osmium isotopic characteristics of mantle-derived rocks. *Geochim. Cosmochim. Acta* 55, 1421–1434.
- Martin, E.E., MacLeod, K.G., Jimenez Berrosoco, A., Bourbon, E., 2012. Water mass circulation on Demerara Rise during the Late Cretaceous based on Nd isotopes. *Earth Planet. Sci. Lett.* 327–328, 111–120.
- McArthur, J.M., Howarth, R.J., Bailey, T., 2004. Strontium isotope stratigraphy. In: Gradstein, F., Ogg, J., Smith, A. (Eds.), *A Geological Time Scale 2004*. Cambridge University Press, Cambridge, UK, pp. 96–105.
- Meisel, T., Walker, R.J., Irving, A.J., Lorand, J., 2001. Osmium isotopic compositions of mantle xenoliths: A global perspective. *Geochim. Cosmochim. Acta* 65 (8), 1311–1323.
- Meyers, S.R., Sageman, B.B., 2004. Detection, quantification, and significance of hiatuses in pelagic and hemipelagic strata. *Earth Planet. Sci. Lett.* 224, 55–72.
- Meyers, S.R., Sageman, B.B., Hinnov, L.A., 2001. Integrated quantitative stratigraphy of the Cenomanian–Turonian Bridge Creek Limestone member using Evolutionary Harmonic Analysis and stratigraphic modelling. *J. Sediment. Res.* 71, 628–644.
- Meyers, S.R., Siewert, S.E., Singer, B.S., Sageman, B.B., Condon, D.J., Obradovich, J.D., Jicha, B.R., Sawyer, D.A., 2012a. Intercalibration of radioisotopic and astrochronologic time scales for the Cenomanian–Turonian boundary interval, Western Interior Basin, USA. *Geology* 40, 7–10.
- Meyers, S.R., Sageman, B.B., Arthur, M.A., 2012b. Obliquity forcing and the amplification of high-latitude climate processes during Oceanic Anoxic Event 2. *Paleoceanography* 27, PA3212. <http://dx.doi.org/10.1029/2012PA002286>.
- Mort, H., Jacquat, O., Adatte, T., Steinmann, P., Follmi, K., Matera, V., Berner, Z., Stuben, D., 2007. The Cenomanian/Turonian anoxic event at the Bonarelli Level in Italy and Spain: Enhanced productivity and/or better preservation?. *Cretaceous Res.* 28, 597–612.
- Oxburgh, R., 2001. Residence time of osmium in the oceans. *Geochim. Geophys. Geosyst.* 2, 2000GC00010.
- Paquay, F.S., Ravizza, G., 2012. Heterogeneous seawater  $^{187}\text{Os}/^{188}\text{Os}$  during the Late Pleistocene glaciations. *Earth Planet. Sci. Lett.* 349–350, 126–138.
- Peucker-Ehrenbrink, B., Ravizza, G., 2000. The marine osmium isotope record. *Terra Nova* 12, 205–219.
- Pogge von Strandmann, P.A.E., Jenkyns, H.C., Woodfine, R.G., 2013. Lithium isotope evidence for enhanced weathering during Oceanic Anoxic Event 2. *Nat. Geosci.* <http://dx.doi.org/10.1038/NGEO1875>.
- Pratt, L.M., Kauffman, E.G., Zelt, F.B., 1985. Fine-grained deposits and biofacies of the Cretaceous Western Interior Seaway: Evidence for cyclic sedimentary processes. *Soc. Econ. Miner. Field Trip Guidebook* 4, 1985 Midyear Meeting, Golden, Colorado.
- Ravizza, G., Peucker-Ehrenbrink, B., 2003. Chemostratigraphic evidence of Deccan volcanism from the marine osmium isotope record. *Science* 302, 1392–1395.
- Robinson, N., Ravizza, G., Coccioni, R., Peucker-Ehrenbrink, B., Norris, R., 2009. A high-resolution marine  $^{187}\text{Os}/^{188}\text{Os}$  record for the late Maastrichtian: Distinguishing the chemical fingerprints of Deccan volcanism and the KP impact event. *Earth Planet. Sci. Lett.* 281, 159–168.
- Sageman, B.B., Meyers, S.R., Arthur, M.A., 2006. Orbital time scale and new C-isotope record for Cenomanian–Turonian boundary stratotype. *Geology* 34, 125–128.
- Schlanger, S.O., Arthur, M.A., Jenkyns, H.C., Scholle, P.A., 1987. The Cenomanian/Turonian Oceanic Anoxic Event, I. Stratigraphy and distribution of organic carbon-rich beds and the marine  $\delta^{13}\text{C}$  excursion. In: Brooks, J., Fleet, A.J. (Eds.), *Marine Petroleum Source Rocks*. In: *Geol. Soc. London Spec. Publ.*, vol. 26, pp. 371–399.
- Selby, D., Creaser, R.A., 2003. Re–Os geochronology of organic rich sediments: An evaluation of organic matter analysis methods. *Chem. Geol.* 200, 225–240.
- Shirey, S.B., Walker, R.J., 1998. The Re–Os isotope system in cosmochemistry and high-temperature geochemistry. *Annu. Rev. Earth Planet. Sci.* 26, 423–500.
- Slingerland, R., Kump, L.R., Arthur, M.A., Fawcett, P.J., Sageman, B.B., Barron, E.J., 1996. Estuarine circulation in the Turonian Western Interior seaway of North America. *Geol. Soc. Am. Bull.* 108, 941–952.
- Smoliar, M.L., Walker, R.J., Morgan, J.W., 1996. Re–Os ages of group IIA, IIIA, IVA, and IVB iron meteorites. *Science* 23, 1099–1102.
- Snow, L.J., Duncan, R.A., Bralower, T.J., 2005. Trace element abundances in the Rock Canyon Anticline, Pueblo, Colorado, marine sedimentary section and their relationship to Caribbean plateau construction and oxygen anoxic event 2. *Paleoceanography* 20, PA3005. <http://dx.doi.org/10.1029/2004PA001093>.
- Takashima, R., Nishi, H., Hayashi, K., Okada, H., Kawahata, H., Yamanaka, T., Fernando, A.G., Mampuku, M., 2009. Litho-, bio- and chemostratigraphy across the Cenomanian/Turonian boundary (OAE 2) in the Vocontian Basin of southeast France. *Palaeogeog. Palaeoclimatol. Palaeoecol.* 273, 61–74.
- Tegner, C., Storey, M., Holm, P.M., Thorarinnsson, S.B., Zhao, X., Lo, C.-H., Knudsen, M.F., 2011. Magmatism and Eureka deformation in the High Arctic Large Igneous Province:  $^{40}\text{Ar}$ – $^{39}\text{Ar}$  age of Kap Washington Group volcanics, North Greenland. *Earth Planet. Sci. Lett.* 303, 203–214.
- Trabucho-Alexandre, J., Tuenter, E., Henstra, G.A., van der Zwan, K.J., van de Wal, R.S.W., Dijkstra, H.A., de Boer, P.L., 2010. The mid-Cretaceous North Atlantic nutrient trap: Black shales and OAEs. *Paleoceanography* 25, PA4201. <http://dx.doi.org/10.1029/2010PA001925>.
- Tsikos, H., Jenkyns, H.C., Walsworth-Bell, B., Petrizzo, M.R., Forster, A., Kolonic, S., Erba, E., Premoli-Silva, I.P., Baas, M., Wagner, T., Sinninghe Damsté, J.S., 2004. Carbon-isotope stratigraphy recorded by the Cenomanian–Turonian Oceanic Anoxic Event: correlation and implications based on three key localities. *Mem. Geol. Soc. Lond.* 161, 711–719.
- Turgeon, S.C., Creaser, R.A., 2008. Cretaceous Anoxic Event 2 triggered by a massive magmatic episode. *Nature* 454, 323–326.
- Voigt, S., Aurag, A., Leis, F., Kaplan, U., 2007. Late Cenomanian to Middle Turonian high-resolution carbon isotope stratigraphy: New data from the Munsterland Cretaceous Basin, Germany. *Earth Planet. Sci. Lett.* 253, 196–210.
- Voigt, S., Erbacher, J., Mutterlose, J., Weiss, W., Westerhold, T., Wiese, F., Wilmsen, M., Woniak, T., 2008. The Cenomanian–Turonian of the Wunstorf section (North Germany): Global stratigraphic reference section and new orbital time scale for Oceanic Anoxic Event 2. *Newsl. Stratigr.* 43, 65–89.
- Wilmsen, M., 2003. Sequence stratigraphy and palaeoceanography of the Cenomanian stage in northern Germany. *Cretaceous Res.* 24, 525–568.
- Yudovskaya, M.A., Tessalina, S.G., Distler, V.V., Chaplygin, I.V., Chugaev, A.V., Dikov, Y.P., 2008. Behaviour of highly-siderophile elements during magma degassing: A case study at the Kudryavy volcano. *Chem. Geol.* 248, 318–341.
- Zheng, X.-Y., Jenkyns, H.C., Gale, A.S., Ward, D.J., Henderson, G.M., 2013. Changing ocean circulation and hydrothermal inputs during Oceanic Anoxic Event 2 (Cenomanian–Turonian): Evidence from Nd-isotopes in the European shelf sea. *Earth Planet. Sci. Lett.* <http://dx.doi.org/10.1016/j.epsl.2013.05.053i>.